Volume 17, Issue 3, 172517 (1-16)

Iranian Journal of Earth Science (IJES)

https://doi.org/10.57647/j.ijes.2025.16800

Petrology of volcanism in the Alasht-Haraz road of the Alborz mountain range, south of Amol (north of Iran)

Reza Elmi[1], Mohammad Ali Arian[1,*], Afshin Ashja Ardalan[1], Abdollah Yazdi[2]

[1]*Department of Geology, NT.C., Islamic Azad University, Tehran, Iran.*
[2]*Department of Geology, Kah.C., Islamic Azad University, Kahnooj, Iran.*

[*]**Corresponding author:** mohamadaliarian049@gmail.com

Original Research

Received:
9 March 2024
Revised:
10 April 2024
Accepted:
27 June 2024
Published online:
10 July 2025

Abstract:

The study area is located in the south and southeast regions of the Amol city, central Alborz mountain range, which is mainly consisted of Mesozoic sedimentary rocks, while cretaceous volcanic rocks are also found at some points of the area. Petrographical studies reveal that these rocks are consisted of basalt, andesite, trachyandesite, trachyte, dolerite, gabbro, and microgabbro, where the hypabyssal rocks are closely related to volcanic rocks through their magma origin. The above mentioned igneous rocks complex are covered with limestone's as Tizkoh Formation. From geochemical point of view, the rocks of the region are of subalkaline and tholeiitic nature, while parts of them are alkaline. Based on petrographical studies, titanium oxides (as opaque minerals) crystallize earlier. The present findings also show that the contents of Al_2O_3 and MgO in comparison to that of SiO_2 follow ascending and descending patterns, respectively. These findings support early partial crystallization of olivine in comparison to plagioclase crystallization in liquidus line phase. Moreover, the descending pattern observed for K_2O and Na_2O in comparison with MgO is also attributed to partial crystallization of the magma and their distribution to some extents is the result of their alteration or contamination with felsic crust materials. Analysis of rock samples normalized to the chondritic values shows gradual enrichment of heavy rare earth elements contents (HREES) compared to those of light rare earth elements contents (LREES). Most of basalts studied in the region are of OIB type. The magmas of basaltic rocks originate from a depth of $100-110$ kilometers and a garnetic lehrzolitic source rock. According to geochemical investigations, the studied rocks originate from the melting of a mantle that undergone magmatic differentiation and is finally polluted with continental crust.

Keywords: Volcanic rocks; Petrology; Alborz mountains; Amol city; Partial crystallization

1. Introduction

The studied area is located in Mazndaran province, on geological maps of Amol and Ghaemshahr. The Alborz mountains as an east-west orogenic belt bordering southern margin of Caspian Sea is part of Alpine-Himalayan ranges (Stöcklin, 1974). The Alborz orogeny recorded significant magmatic and tectonic events mainly after Cimmerian microcontinents-Eurasia suturing (Alavi, 1996; Zanchi et al., 2009; Ghasempour et al., 2015; Arjmandzadeh et al., 2020; Mollai et al., 2021; Ashrafi et al., 2024; Salehpour et al., 2025). During the Late Cretaceous, voluminous volcanic rocks crop out in Alborz (Fig. 1). The most important villages in this region are Neshel, Filband, Sangchal, Lerzaneh, Sheikh Musa, Nirasem, Akhen Sar, Pashakla, Alamestan, Shah Zeyd Savadrudbar, Mangal, and Lakum along with several other small villages. The Alborz Mountains are part of the Alpine-Himalayan orogenic belt and have formed due to the convergence of Central Iran and Eurasia from the late Triassic. In Iran, these structures are divided into Eastern Alborz, Central Alborz and Western Alborz. The maximum elevation of the study area is 3587 meters above the sea level (m.a.s.l.) in Zardsar mountain, while the lowest point is located in the southeast of the region in Haraz valley with an altitude of 700 m.a.s.l. Several peaks higher than 3500 m (e.g., Deh Posht mountains, Sang-ePol, Ghangiz, Damkesh, and Sard-Khouni) are also seen in this area. Tectonic activities and abundant faults have caused height differences in this rectangle. Early Cretaceous and Late Cretaceous volcanic rocks are exposed

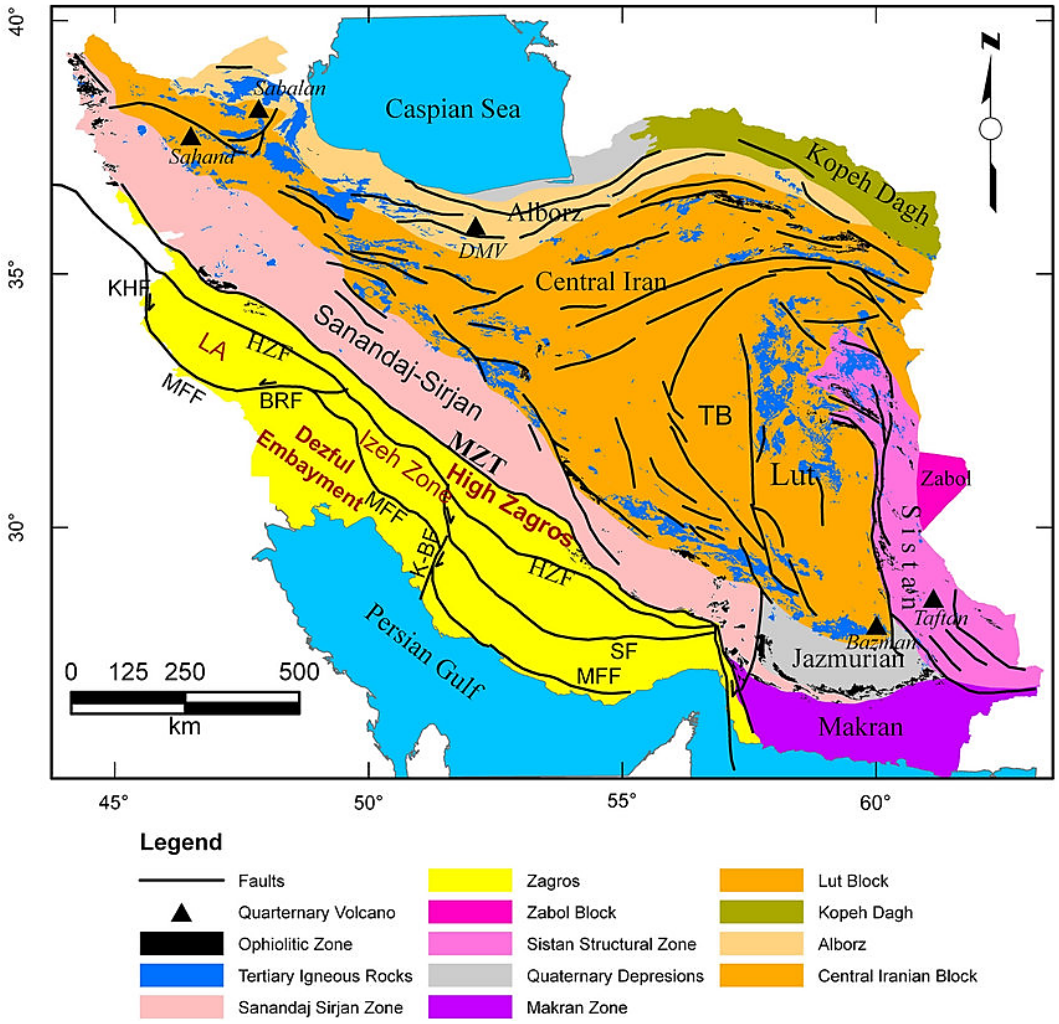

Figure 1. Tectonic sedimentary zone of Iran (Teknik and Ghods, 2017). The study area is shown by a blue rectangle.

in the studied quadrangle. These rock units are underlain by Triassic, Jurassic, and Cretaceous sedimentary rocks (Assereto, 1966; Sarem et al., 2021). Due to the relatively high Resistance to erosion of these rocks, the morphology of this area has a rougher shape, and the formed heights are along with valleys with a vertical wall and many faults. This altitude difference can be attributed to erosion, tectonic movements, and abundant faults. Alluvial sediments along rivers and alluvial fan sediments at slopes of some altitudes are other geomorphological features of the study area. In addition, this area has several catchment basins, and since rivers are rapidly affected by tectonic activities, the impact of these activities is reflected in the catchment basin and its geomorphology.

2. Geology of the study area

The study area is located in the south and southeast of Amol city in the Mazandaran province (Iran) on geological map of Amol and Ghaemshahr (Fig. 2). Along the Haraz road, 120 km from Tehran to Amol, we reach Baijan village. After 25 km, through a mountainous road, we have Neshel village. An asphalt sideroad with a length of 7 km is branched from Baijan village. Eventually, we reach the study area after passing the 18-km-long mountainous road. The study area is located in the longitude of 52° 15′ to 53° 00′E and latitude of 36° 00′ to 36 15′N with a surface area of 1800 km^2. Amol city is located in the northwest and outside the area, and Alasht is in the southeast and within the study area. First, the 1:100,000 Ghaemshahr map (Vahdati Daneshmand and A., 2003) and Amol Geology map (Vahdati Daneshmand, 1999) maps covering the study area were obtained. Next, the 1:25,000 and 1:50,000 topographic maps of the area were collected. For petrographic studies of thin rock samples taken during field operations, a total of 210 rock samples were taken from the whole area during two months of fieldwork. The results of 10 chemical analyses (Elmi and Arin, 2015) related to previous studies were also used as supplementary data.

Thin sections were prepared from fresh samples and studied using polarized light microscopy technique and appropriate samples were selected for chemical analyses. Consequently, 14 samples were analyzed in Zarazma Laboratory using the Lithium Fusion method for the main oxides. In this method, metaborate decomposes most of the refractory elements and can decompose the main oxides.

Combining this method with LOI volatiles determines the overall composition of the rock. In this technique, the sample is melted using lithium metabolite, the melted prod-

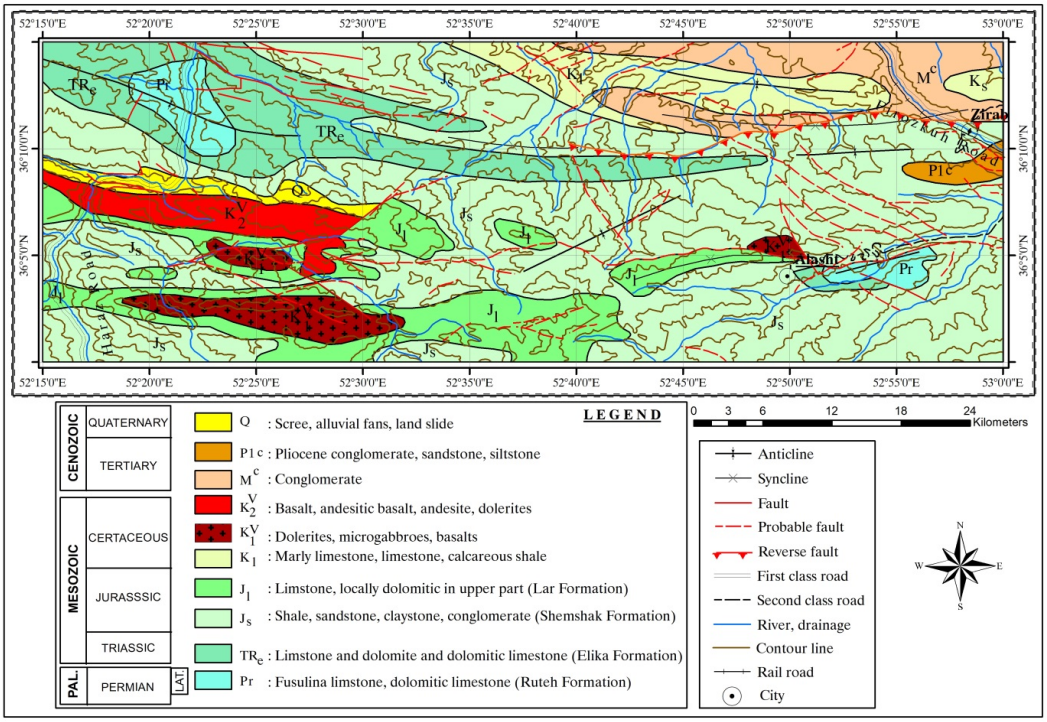

Figure 2. Geological map of the research area based on previous reports, (Vahdati Daneshmand and A., 2003) and (Vahdati Daneshmand, 1999).

uct is dissolved using dilute nitric acid. Then, the final solution was read using the Inductively Coupled Plasma-Optical Emission Spectrometry (ICP-OES) equipment, and the amount of the main oxides was determined. Furthermore, the trace elements (at least 56 elements) were studied using the four-acid analysis method and ICP-MS readings. It is noteworthy that the percentage of oxides obtained from these chemical decompositions is used in petrological studies and various chemical classifications.

Early Cretaceous and Late Cretaceous volcanic rocks were subjected to geochemical and petrogenesis studies. Early Cretaceous volcanic rocks (more precisely, Neocomian) are a maximum of 300 m thick and mainly include dolerite, basalt, basaltic andesite, and pyroclastic rocks. Eruptions of most of the mentioned lavas have occurred in the terrestrial environment. These lavas are overly Neocomian rocks (Early Cretaceous), and are overlain by limestone's of the Tizkooh Formation belonging to the Late Cretaceous. Therefore, according to their stratigraphic position, they are Early Cretaceous in age and, more precisely, Middle to Upper Neocomian. The extensions caused by the Late Cimmerian events have led to extensive volcanic eruptions in the area. As a result, alkaline and sometimes moderate volcanic rocks, as well as related pyroclastic, have considerably increased in the southern parts of the study area from Larzaneh to Neshel and also in Amol sheets. One kilometer north of Lakum and in the fault contact with limestones of Lar Formation, lavas have penetrated to some extent, and fragments of limestone are seen in them, suggesting the younger age of volcanoes. This unit has reached a thickness of 50 to 100 m in the core of the Neshel syncline. Also, they are located on gypsums and dolomites of Neocomian units with erosional unconformity. According to palaeogeographic reconstructions (Stöcklin, 1974; Stampfli et al., 1991; Saidi et al., 1997; Besse et al., 1998; Stampfli and Borel, 2002), the Iranian microplate was the first block to collide with Eurasia during Middle-Late Triassic forming the Eo-Cimmerian orogeny. This event is recorded by a low-angle regional angular unconformity (Stöcklin, 1974; Jenny and Stampfli, 1978) along the northern margin of the Iranian plate, sealed by the Upper Triassic-Jurassic Shemshak Formation (Assereto, 1966; Seyed-Emami, 2003). A Permo-Triassic accretionary-subduction complex marking the Paleotethys suture between the Turan and the Iranian plate has been recognized in the Mashad and Torbatjam regions to the east (Ruttner, 1993). Tentatively traces the Paleotethys suture westward across the Gorgan region to the Talesh mountains (western Alborz), where metamorphic nappes (Clark et al., 1975; GSI, 1997) are uncomfortably covered by the Shemshak Formation.

The record of the Eocimmerian orogeny is less evident in the central part of the Alborz. The Upper Triassic succession is almost continuous (Ghasemi Nejad et al., 2004; Dabiri et al., 2018) and is marked by a sudden change in sedimentation, from shallow sea carbonates to sandstones, suggesting that central Alborz was located south of the main suture zone and then behaved as a stable foreland region during the collision.

In synclines of the south of Filband, the Tizkooh Formation overlay them with an erosional unconformity. Therefore, their age is estimated to be middle to late Neocomian. The formation also consists of melaphyre rocks, in which a large amount of carbonate decomposition and poor stratification is seen. In addition, they are often penetrated by numerous

black diabase microgabbro dikes at slightly younger ages. Sequences of black lava, sometimes dark gray, green, and red, are seen with pyroclasts, tuffs and sometimes lapilli-tuffs. Vertical tectonic movements have intensified during the Cretaceous and been accompanied by volcanic activity at some intervals. In the study area, Late Cretaceous volcanic rocks can be divided into lower and upper parts. Lower Cretaceous volcanic rocks are denoted by k_2^v in the geological map of Amol (Fig. 2). This section is about 200 m thick in the west of Panjab village, and its igneous section includes mass dolerites. The age of this volcanic unit is Cenomanian due to the fossilized limestones overlying and overlain by them. The volcanic rocks of the upper Late Cretaceous with the sign k_2^v can be seen on the 1:100,000 map of the Amol rectangle (Fig. 2). Its thickness is measured to be 200 to 312 m, and it is comprised of basalt rocks, andesite basalts, pyroxene andesite, trachy andesite, trachyte, and a little of pyroclastic rocks. Along with these volcanic rocks, overlain by limestone and marly limestone of the Late Cretaceous. Based on petrographic studies in this rectangle, the following igneous rocks exist in this map: 1-Olivine basalt, 2-Basalt, 3- Andesite, 4-Trachyandesite, 5-Trachyte, 6- Dolerite, 7-Gabbro.

3. Petrography and analytical methods

During the field study, 210 samples were taken, and then thin sections were prepared. The samples were among the fresh outcrops and the weathered rims of the samples were removed, before packing in plastic sample bags. They were studied by polarizing microscope at the North Tehran Branch of Islamic Azad University, using a standard method for the classification of igneous rocks (Streckeisen, 1979). Twenty four samples were analyzed in Zarazma Laboratory using Lithium Borate Fusion and Inductively Coupled Plasma-Mass Spectrometry methods (ICP-MS) for whole-rock major and trace-element analyses.

3.1 Olivine basalts

Olivine basalts are more abundant in the south and southeast of the studied rectangle. The color of olivine basalts in the hand sample is dark green-dark gray or black and has some fractures due to tectonic stresses. The textures of olivine basalts include porphyritic, microlithic porphyritic, hyalo porphyritic, glomero porphyritic, and ophitic. Rock matrix varies from glass to very fine crystalline and microlithic. Phenocrystals include olivine, augite pyroxene, and plagioclase, which are the main minerals of the rock. Also, rock pores are filled with phenocrysts, fine augite, magnetite, plagioclase, rutile, and sphene crystals (Fig. 4 (a)).

3.2 Basalt

Basalts are more abundant in the southeast and center of the study area, especially near the villages of Serin and Lakum (Fig. 3 (a)). These rocks are in the form of lava flows and are associated with olivine basalt. In the hand sample, they are porous masses with cavities filled with secondary minerals. Their weathering surface is light brown, and the fresh surface is gray to black. They have porphyritic hyaloporphyritic and microlithic textures. Also, the rock matrix consists of opaque minerals, glasses and a small amount of microlithic plagioclase and olivine phenocrysts. Sometimes, cavities are found in basalts filled with zeolite or calcite (Fig. 4 (b)).

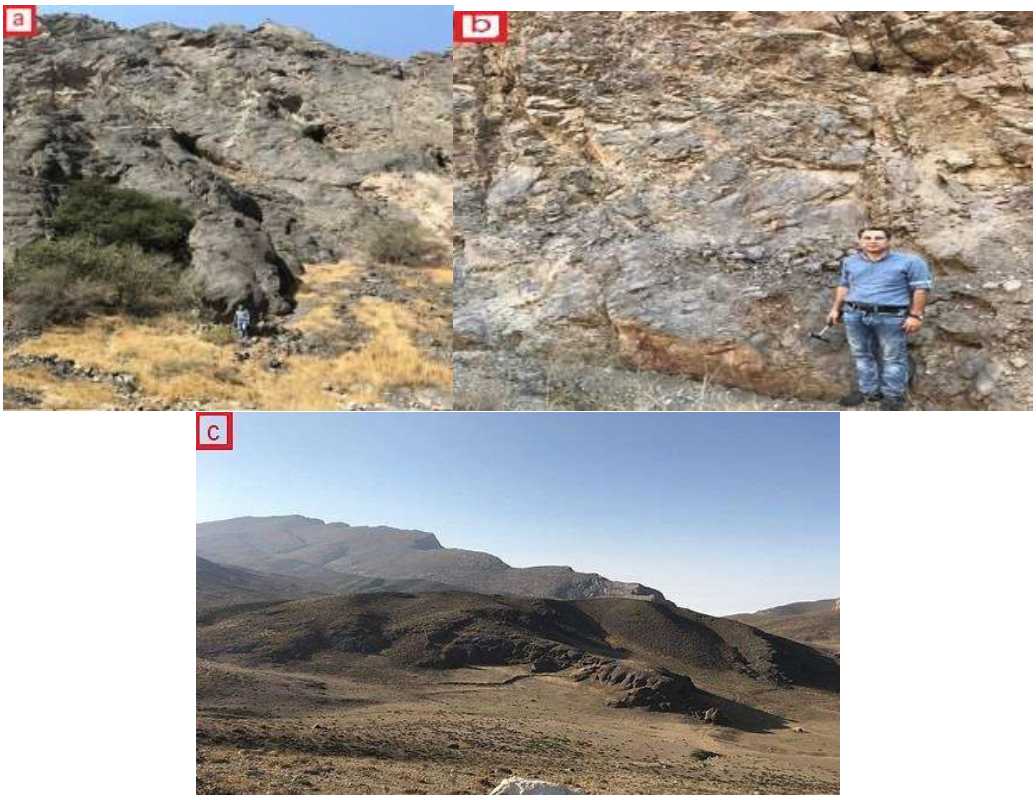

Figure 3. (a) Field photograph of the basalt. (b) Field photograph of the andesite. (c) Field photograph of the dolerite.

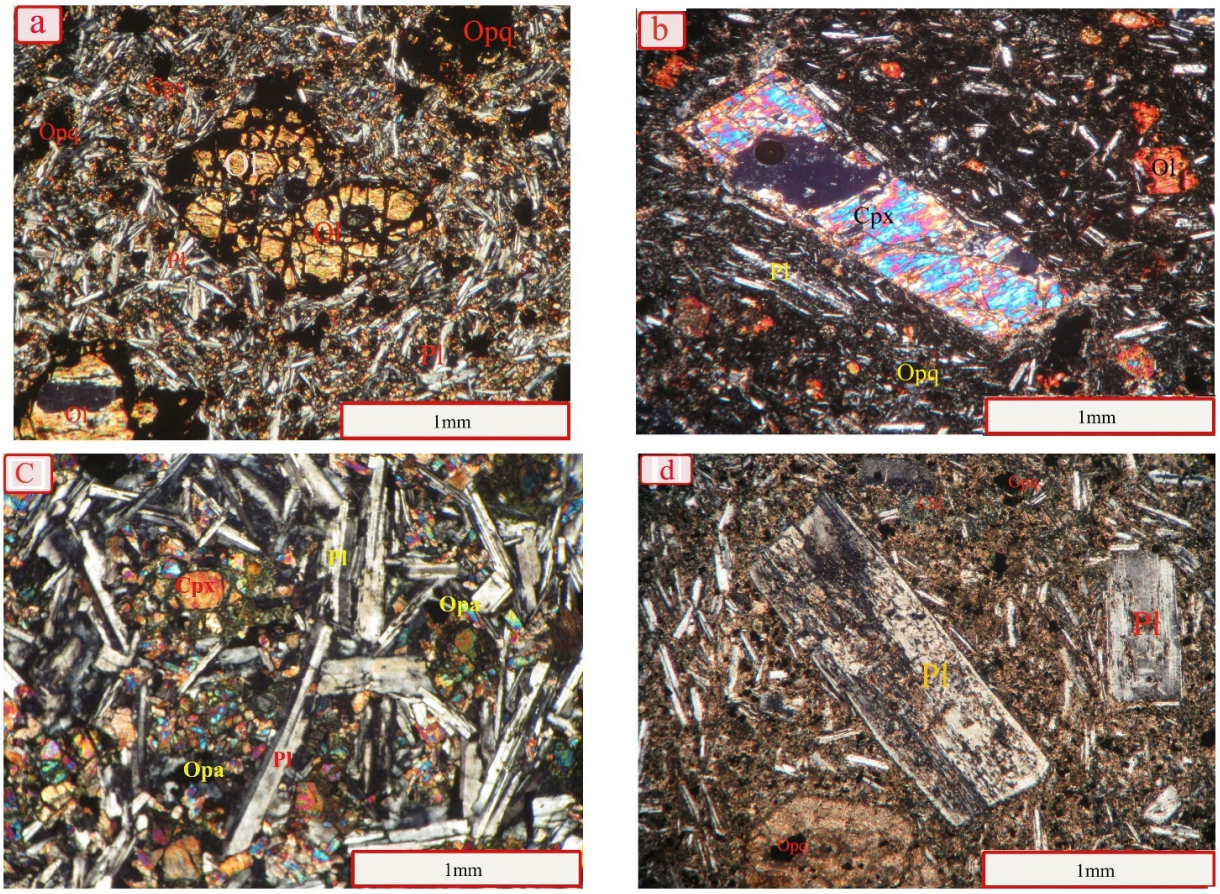

Figure 4. (a) Plagioclase and pyroxene crystals in olivine basalts (XPL). (b) Euhedral and subhedral plagioclase crystals and pyroxene minerals in basalts (XPL). (c) Euhedral and subhedral plagioclase crystals and opaque minerals in dolerite (XPL). (d) Altered plagioclase and opaque minerals in andesite (XPL).

3.3 Dolerite

Dolerite, observed in some basic masses, is located as dikes in the semi-deep sections of volcanic massives. Their weathered color is dark green to black (Fig. 3 (c)). The texture of these rocks is intersertal and is microlitic porphyritic in some parts of the thin sections. Rock phenocrysts include olivine, augite, and plagioclase. The plagioclases are angled relative to each other, with olivine, augite, and opaque mineral crystals on their sides (Fig. 4 (c)).

3.4 Andesite

Andesites have formed outcrops and low-height mountains in the west and northwest of the studied rectangle. In the hand sample, they are gray to brown. The white and euhedral feldspar crystals, which are geometrically rectangular, are placed in a homogeneous matrix where only white microlits are visible. Some microlitic porphyritic texture is found in these rocks, with their main mineral being plagioclase. This colorless euhedral mineral has three series of the good, medium, and weak cleavages. Plagioclase is an andesine type with a maximum extinction angle of 24°. Plagioclase phenocrysts are contained in a glassy or very fine crystal matrix, although plagioclase microliths and opaque minerals can also be detected in this matrix. Opaque minerals make up 7% of the rock and are seen as fine crystals in the rock matrix. The maximum dimensions of these minerals reach 0.5 mm. In some andesites of the study area, pyroxene augite is also found in the rock matrix. The secondary minerals of calcite are generated due to the plagioclase degradation and scattered in cavities and rock fractures. The rate of andesite alteration is moderate, although they have intense alterations in some samples (Fig. 4 (d)).

3.5 Trachyandesite

Trachyandesites exist in smaller amounts with andesites and trachyte in the western half of the study area. These rocks appear in light gray in the hand sample. The texture of most of these trachyandesites is microlithic porphyritic and is porous in some samples. The main minerals include plagioclase and orthoclase. Sericite and hematite are also secondary minerals of the rock (Fig. 5 (a)).

3.6 Trachyte

Trachytes were along with trachyandesite (with less expansion and more limited outcrops) in the western parts and generally in the western half of the study area. These rocks appear in small masses and completely in the form of rocks associated with trachyandesites. In the hand sample, they are dense with high strength and are light gray in color. Rock minerals include orthoclase, opaque minerals, sericite, and calcite (Fig. 5 (b)).

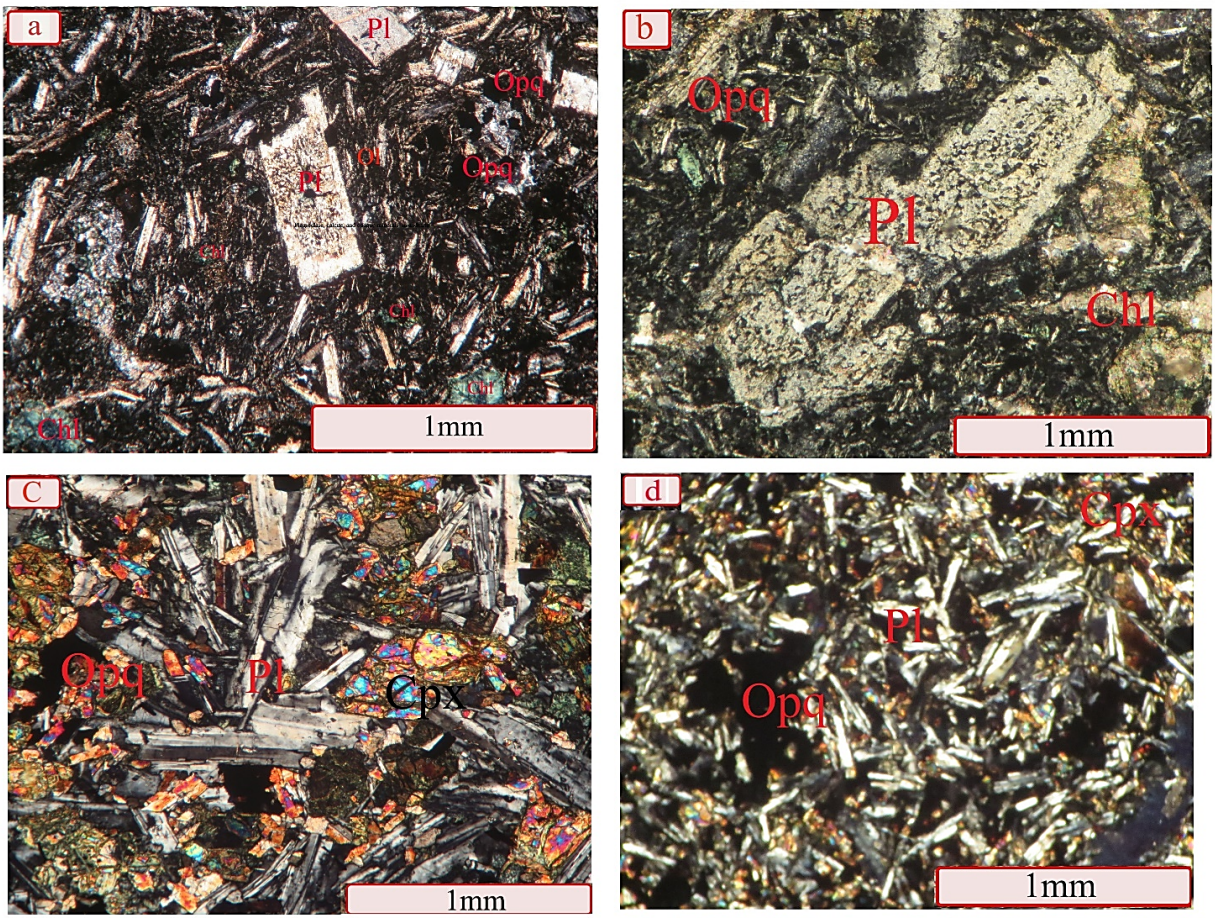

Figure 5. (a) Texture of microlithic porphyritic in trachyandesites (XPL). (b) Decomposed plagioclase and opaque minerals in trachyte (XPL). (c) Granular textures in gabbro (XPL). (d) Micro intergranular textures in microgabbro (XPL).

3.7 Gabbro

The same basaltic magma making the whole studied mass has formed the gabbro rock due to cooling at a larger depth. In the hand sample, its color is dark green to black and has intergranular and granular textures. The rock's plagioclase crystals are medium-sized up to 2 mm long, and mainly appear as euhedral and rarely as subhedral crystals (Fig. 5 (c) and 5 (d)). Also, among the plagioclase minerals, some relatively iddingsitized subhedral olivine phenocrysts and healthy euhedral to subhedral augite minerals are seen. The accessory minerals of these rocks are rutile and opaque minerals. Rutile is reddish-brown and appears as fine or needle-shaped prismatic crystals in thin sections. It has a very strong relief, and its birefringence is not seen completely due to light reflection. Moreover, this mineral has a direct extinction.

4. Geochemistry of rocks in the study area

For the geochemical study of volcanic rocks in the study area, 24 samples with the least amount of alteration were selected, and the whole rock was chemically analyzed. Chemical analysis was performed by the alkali fusion method for the main elements, volatiles, and by ICP-MS and ICP-EOS methods for some rare earth elements (REEs) and other accessory elements (Tables 1- 3). In the $Na_2O + K_2O$ vs SiO_2 diagram (Le Bas et al., 1986), the studied volcanic rocks have the composition of basalt, basaltic andesite, basaltic trachyandesite, trachyandesite, andesite, and trachyte (Fig. 6 (a)) and are in the sub-alkaline and alkaline series (Fig. 6 (b)). In addition, in the $Na_2O + K_2O$ vs. SiO_2 diagram (Cox et al., 1979), these rocks are placed in the combined range of basalt, basaltic andesite, trachyandesite, andesite, and trachyte (Fig. 6 (b)). The location of the specimens near the line separating the sub-alkaline and alkaline basalts, along with the petrographic evidence, indicate the basic and intermediate rocks have different nature magma forming these rocks.

According to the $Na_2O + K_2O$ vs SiO_2 diagram (Irvin and Baragar, 1971), the samples of the study area are in the sub-alkaline and alkaline range, basaltic rocks are subalkaline and intermediate rocks are alkaline (Fig. 6 (c)).

Based on the ternary FeO*-($Na_2O + K_2O$)-MgO diagram (Irvin and Baragar, 1971), sub-alkaline samples are in the range of calc-alkaline series (Fig. 6 (d)). In this diagram, basaltic rocks are mostly located at the tholeiite-calc-alkaline boundary. However, the intermediate rocks (andesite, trachyandesite and trachyte) show the calc-alkaline trend due to their more crustal contamination (CC). The calc-alkaline series is derived from both primary and secondary sources, which are likely to be secondary rocks in the area of origin (CC). The elements in some of these diagrams do not represent trends with specific petrological

Table 1. The results of chemical analysis of major elements of the rocks of the studied area.

Element	SiO_2	Al_2O_3	BaO	CaO	FeO	K_2O	MgO	MnO	Na_2O	P_2O_5	SO_3	TiO_2	Cr_2O_3
E.106	47.656	15.307	0.053	9.798	13.604	1.398	6.718	0.210	2.460	0.463	0.095	2.187	0.053
E.107	47.329	15.021	0.052	10.189	13.152	1.551	7.160	0.189	2.159	0.461	0.000	2.684	0.052
E.108	46.641	13.478	0.000	8.972	12.644	0.787	11.386	0.186	2.922	0.466	0.093	2.372	0.052
E.110	47.510	15.462	0.000	10.108	13.909	1.336	6.532	0.137	2.430	0.431	0.000	2.146	0.000
E.124	46.679	13.239	0.052	8.667	12.649	1.102	12.917	0.187	2.037	0.468	0.000	1.943	0.062
E.132	46.849	14.624	0.053	10.268	12.835	1.284	7.985	0.221	2.630	0.652	0.000	2.546	0.053
E.150	62.247	17.405	0.000	0.184	7.090	5.730	0.174	0.255	6.425	0.000	0.072	0.419	0.000
E.160	53.691	18.566	0.000	5.312	9.992	2.039	2.264	0.161	4.604	0.569	0.107	2.694	0.000
E.165	51.495	19.285	0.065	7.526	8.974	2.753	2.203	0.238	4.319	0.540	0.000	2.602	0.000
E.170	63.624	16.392	0.360	2.502	5.342	4.716	0.113	0.134	6.044	0.072	0.165	0.535	0.000
E.173	62.224	19.314	0.103	0.760	5.103	5.319	0.739	0.072	5.411	0.164	0.000	0.791	0.000
E.179	53.421	18.907	0.116	3.847	9.188	3.393	2.160	0.126	5.828	0.548	0.000	2.466	0.000
E.184	54.996	18.894	0.105	3.678	8.512	3.825	2.287	0.105	4.594	0.495	0.053	2.455	0.000
E.200	44.773	15.618	0.000	10.634	11.922	0.729	9.155	0.158	2.862	0.729	0.053	3.305	0.063
E.45	46.695	13.907	0.000	10.979	12.500	0.944	9.505	0.116	2.312	0.693	0.001	2.349	0.000
E.51	47.072	13.784	0.000	8.822	13.058	0.866	10.544	0.308	2.235	0.577	0.022	2.712	0.000
E.43	48.119	13.107	0.000	10.952	11.931	0.976	9.796	0.128	2.133	0.596	0.017	2.244	0.000
E.29	52.264	14.695	0.000	8.562	11.001	1.810	6.112	0.276	2.771	0.417	0.008	2.084	0.000
E.34	51.335	14.906	0.000	8.268	10.346	1.944	7.296	0.365	2.801	0.466	0.006	2.265	0.000
E.27	51.301	15.042	0.000	8.435	11.189	2.001	6.058	0.093	2.959	0.507	0.012	2.404	0.000
E.24	49.155	14.536	0.000	9.984	12.860	1.814	6.135	0.124	2.349	0.685	0.016	2.343	0.000
E.23	48.019	14.807	0.000	7.921	13.480	0.897	8.722	0.279	2.551	0.493	0.018	2.812	0.000
E.28	50.118	15.090	0.000	8.074	12.119	1.333	8.201	0.257	2.529	0.292	0.010	1.976	0.000
E.31	52.165	15.191	0.000	8.327	11.279	1.962	5.628	0.081	2.866	0.405	0.008	2.088	0.000

implications. This lack of trend is attributed to the short period of silica oxide changes in the rocks of the region and the greater mobility of the main elements during the secondary processes. The trend of Na_2O against SiO_2 is ascending, suggesting fractional crystallization (FC). Nevertheless, their scattering pattern can be interpreted by Na mobility due to alteration and CC. The trend of Al_2O_3 vs SiO_2 is descending, which seems natural due to the presence of Ca and Al-rich plagioclases in the basaltic to intermediate types (Fig. 7).

However, some of the observed scatterings are also related to the frequency of plagioclase phenocrysts. The chemical discontinuity or gap seen in the relevant Harker diagrams can be attributed to the introduction of large volumes of new magma into the magma chamber or the segregation of the residual fluid of the FC. The concentration range of Na_2O variation varies from 2.13% in the olivine basalts to 6% in the trachyte. This high concentration of Na_2O in the basaltic rocks of this region is somewhat consistent with the rocks of continental rift areas that contain 3.55% Na_2O (Gill, 2010).

K_2O vs SiO_2 indicates an ascending trend, probably due to the FC, and has less dispersion than Na_2O. Significant trends are observed in the diagrams of this range. As two immobile elements, P and Ti show an increasing trend with a decrease in MgO concentration. Also, the ascending trend of TiO_2, which is accompanied by the ascending trend of MgO concentration, provides petrographic evidence of the early crystallization of titanium oxides (as opaque phases) in the region's rocks. The ascending trend of Al_2O_3 and SiO_2 vs MgO indicates the partial crystallization of early olivine compared to the plagioclase crystallization in the liquidus phase. The descending trend of K_2O and Na_2O vs MgO also shows the partial crystallization of the magma, and their scattering is partly the result of relative alteration or contamination with felsic crustal materials. La, Ce, Dy, Sm, Nd, Yb, and Lu have linear and positive trends against Zr and Th, while REEs and compatible elements Co and Ni show a negative trend (Fig. 8).

The trends observed in these diagrams show the affinity of the region's rocks and the origin of the magma that causes their formation from a source with almost similar geochem-

Table 2. Representative whole rock analysis of the rocks for rare elements (ppm).

Element	E.106	E.107	E.108	E.110	E-.124	E.132	E.150	E.160	E.165	E.170	E.173	E.179	E.184
Ag	0.5	0.6	0.5	0.5	0.5	0.7	0.9	0.9	1.1	0.9	0.9	1.1	1
As	8.1	8	4.7	8.1	5.6	6	3.8	1.8	1.4	1	3.3	2.4	5.4
Ba	357	366	295	332	359	397	62	266	466	2366	724	866	788
Be	0.9	1.1	1.1	0.9	0.9	1.1	5.7	3.3	2.5	1.7	3.1	4.1	3.6
Bi	0.1	0.1	0.1	0.1	0.1	0.1	0.1	0.1	0.1	0.1	0.1	0.1	0.1
Cd	0.1	0.1	0.1	0.1	0.1	0.1	0.1	0.1	0.1	0.1	0.1	0.1	0.1
Ce	56	52	52	50	53	68	241	100	103	103	112	108	107
Co	42.2	45	46.8	38.2	47.3	41.5	1.8	18.4	16.7	2.3	2.8	14.3	14.5
Cr	272	334	313	306	345	324	16	31	54	17	10	17	17
Cs	0.5	0.5	0.5	0.5	0.5	0.5	0.5	0.7	0.9	0.5	0.6	0.6	1
Cu	54	53	91	44	79	108	9	29	25	15	15	7	15
Dy	5.24	5.75	5.2	4.82	4.73	4.98	7.44	6.31	5.69	5.38	4.84	6.18	6.5
Er	2.28	2.18	1.93	2.07	1.88	2.35	3.55	2.59	2.85	2.13	2.33	2.51	2.73
Eu	1.93	2.17	1.89	1.6	1.64	2.18	0.54	2.05	2.86	4.43	2.36	2.75	2.95
Gd	5.12	4.92	4.72	4.45	4.58	5.56	10.6	6.22	6.45	5.21	5.09	6.39	6.89
Hf	3.75	4.74	4.56	3.64	3.58	5.2	8.22	7.93	6.01	7.2	6.23	7.35	8.63
In	0.5	0.5	0.5	0.5	0.5	0.5	0.5	0.5	0.5	0.5	0.5	0.5	0.5
La	32	27	25	26	28	36	110	47	49	48	54	52	51
Li	7	10	11	6	18	6	1	19	16	6	7	14	18
Lu	0.38	0.29	0.34	0.33	0.32	0.34	0.42	0.41	0.53	0.5	0.31	0.38	0.44
Mn	1255	1115	1136	834	1185	1377	1762	1040	1485	788	497	833	715
Mo	2	2	2	1	1	2	3	3	2	6	2	2	1
Nb	29.2	19	18.6	12.5	18.4	20.6	51.6	19.3	15.8	43.5	46.3	27.9	30.8
Nd	26.3	27.9	26.1	23.3	25.2	33	95.4	42.1	42.5	32.6	35.1	45.2	43
Ni	217	184	254	220	313	250	4	16	15	9	1	11	5
P	1620	1768	1737	1618	1630	2293	132	2109	1838	358	601	1895	1841
Pb	5	11	15	10	7	3	23	9	186	5	7	4	13
Pr	6.96	7.2	7	6.38	6.59	9.09	28.71	11.97	12.33	10.88	10.72	12.3	12.12
Rb	1	1	1	1	1	2	86	19	29	22	34	30	43
S	219	71	75	51	69	53	233	121	153	398	50	131	84
Sb	0.5	0.6	0.5	0.5	0.5	0.5	0.5	0.5	0.5	0.5	0.5	0.5	0.5
Sc	21	22	18.4	21.2	19.3	21	0.6	10.2	9.8	3.6	3	9.7	9.9
Se	1.41	1.08	0.5	0.5	0.5	0.5	2.02	0.5	0.5	1.72	1.69	2.34	0.5
Sm	5.48	6.02	5.54	5.38	5.31	7.22	13.94	8.41	8.75	10.27	6.15	9.16	8.91
Sn	1.5	1.4	3.7	0.7	0.8	0.8	10.2	2.2	2	2.5	3	2.6	2.8
Sr	501	586	611	516	520	680	26.9	393	662	457	201	402	364
Ta	1.59	0.42	0.36	0.26	0.71	0.6	0.73	0.58	0.66	2.8	2.53	1.47	1.26
Tb	0.8	0.88	0.84	0.84	0.79	0.91	1.51	1.09	1.03	0.81	0.72	1.14	1.06
Te	0.1	0.13	0.1	0.1	0.1	0.1	0.1	0.1	0.1	0.1	0.1	0.1	0.1
Th	4.6	5	4.7	4.9	4.9	5.3	8.1	5.8	6.9	5.9	5.2	6.2	5.9
Tl	0.1	0.1	0.1	0.1	0.1	0.1	0.25	0.1	0.1	0.1	0.1	0.1	0.1
Tm	0.33	0.29	0.28	0.32	0.3	0.36	0.43	0.34	0.45	0.42	0.36	0.38	0.46
U	0.9	0.9	0.8	0.7	1	1.2	1.6	2.6	2	0.9	1.7	1.4	1.5
V	205	224	191	207	183	208	11	136	125	12	13	110	112
W	1	1	1	1	1	1	1	1	1	1.3	1	1	1
Y	17.9	17.2	15	17.4	15.3	18.3	24.6	22.3	22.5	24.5	23.5	23.3	23.9
Yb	2.1	2	1.7	2.1	1.8	2	2.3	2.3	2.3	2.6	2.1	2.5	2.4
Zn	129	123	129	140	122	129	242	100	132	12	81	126	145
Zr	139	148	152	137	132	178	386	384	368	420	438	428	453

Table 3. Representative whole rock analysis of the rocks for rare elements (ppm).

Element	E.200	E.45	E.51	E.43	E.29	E.34	E.27	E.24	E.23	E.28	E.31
Ag	0.7	0.7	0.9	0.85	0.7	0.7	0.9	0.85	0.7	0.7	0.9
As	6.1	21	7	19	34	102	31	63	55	11	158
Ba	537	782	690	725	635	737	663	782	804	564	569
Be	1.3	1.2	1.20	1.3	1.2	1.20	1.3	1.2	1.20	1.3	1.2
Bi	0.1	0.1	0	0.2	0.1	0	0.13	0.2	1.3	1.2	1.20
Cd	0.1	0.1	0.1	0.1	0	0.1	0.1	0	0.1	0	0.1
Ce	78	289	228	376	180	139	175	221	146	248	149
Co	30.1	8	5	11	9	9	7	7	5	6	9
Cr	255	289	228	376	180	139	175	221	146	248	149
Cs	1.8	1.99	2.02	1.8	1.99	2.02	1.8	1.99	2.02	1.8	1.99
Cu	71	57	59	42	79	68	47	35	46	90	52
Dy	5.99	5.36	5.23	4.56	5.33	5.36	5.66	4.65	5.02	5.20	5.10
Er	2.24	2.33	2.66	2.45	2.55	2.33	2.34	2.45	2.57	2.75	2.66
Eu	2.51	2.63	2.36	2.66	3.23	3.65	3.78	3.77	4.20	4.23	4.25
Gd	6.47	4.52	3.56	2.35	4.56	4.69	6.4	6.5	5.45	5.32	3.25
Hf	5.95	5.30	5.50	5.20	5.55	5.24	5.20	6.5	4.75	5.20	5.23
In	0.5	0.45	0.32	0.33	3.35	3.45	3.4	3.55	3.66	0.24	0.23
La	36	24	19	22	17	26	32	18	28	24	27
Li	26	25	24	27	25	24	26	25	24	28	25
Lu	0.32	0.32	0.35	0.40	0.25	0.36	0.36	0.25	0.24	0.14	0.25
Mo	2	1	2	2	4	6	4	2	1	1	3
Nb	25.1	1	2	1	2	4	2	1	3	2	4
Nd	39.9	31.65	32.9	31.65	38.9	29.65	29.45	23.65	28.9	27.65	29.19
Ni	118	281	246	339	154	146	121	166	196	259	152
P	2481	2455	2433	2566	2633	2544	2366	3245	2780	2456	2450
Pb	1	5	12	12	5	31	5	5	11	8	9
Pr	10.58	11	10.5	12.22	12.30	11.54	12.46	13.25	10.23	10.25	11.45
Rb	1	15	14	16	31	30	29	29	18	23	32
S	73	72	70	72.5	70.45	71.5	72	73	71.35	72.36	71.35
Sb	0.6	0.5	0.5	0.6	0.35	0.66	0.5	0.45	0.35	0.66	0.5
Sc	23.4	22.3	20.36	20.65	23.45	24.56	25.78	27.45	22.14	22.36	22.36
Se	0.5	0.45	0.25	0.45	0.5	0.45	0.25	0.45	0.5	0.56	0.55
Sm	8.45	7.55	8.69	8.56	8.35	7.68	7.70	6.75	6.89	7.56	7.66
Sn	1	1	1	1	1	1	1	1	1	1	1
Sr	716	908	858	702	606	620	692	697	861	416	645
Ta	0.55	0.55	0.65	0.68	0.98	0.25	0.45	0.66	0.78	0.95	0.75
Tb	0.92	0.88	0.98	0.75	0.66	0.45	0.63	0.78	0.88	0.65	0.79
Te	0.1	0.1	0.1	0.2	0.1	0.2	0.1	0.2	0.1	0.2	0.1
Th	4.7	2	1	1	1	1	1	2	1	3	2
Tl	0.1	0.1	0.1	0.1	0.1	0.1	0.1	0.1	0.1	0.1	0.1
Tm	0.37	0.36	0.45	0.34	0.37	0.36	0.45	0.34	0.37	0.36	0.45
U	0.9	2	1	1	1	1	1	2	1	3	2
V	241	240	282	238	248	252	240	243	285	240	242
W	1	4	2	1	1	2	4	3	2	4	2
Y	19.6	14	11	15	18	21	17	16	12	15	19
Yb	2.2	0	0	0	0	0	0	0	0	0	0
Zn	95	78	92	113	86	89	81	81	98	89	84
Zr	211	186	157	142	134	131	124	121	134 119 128		

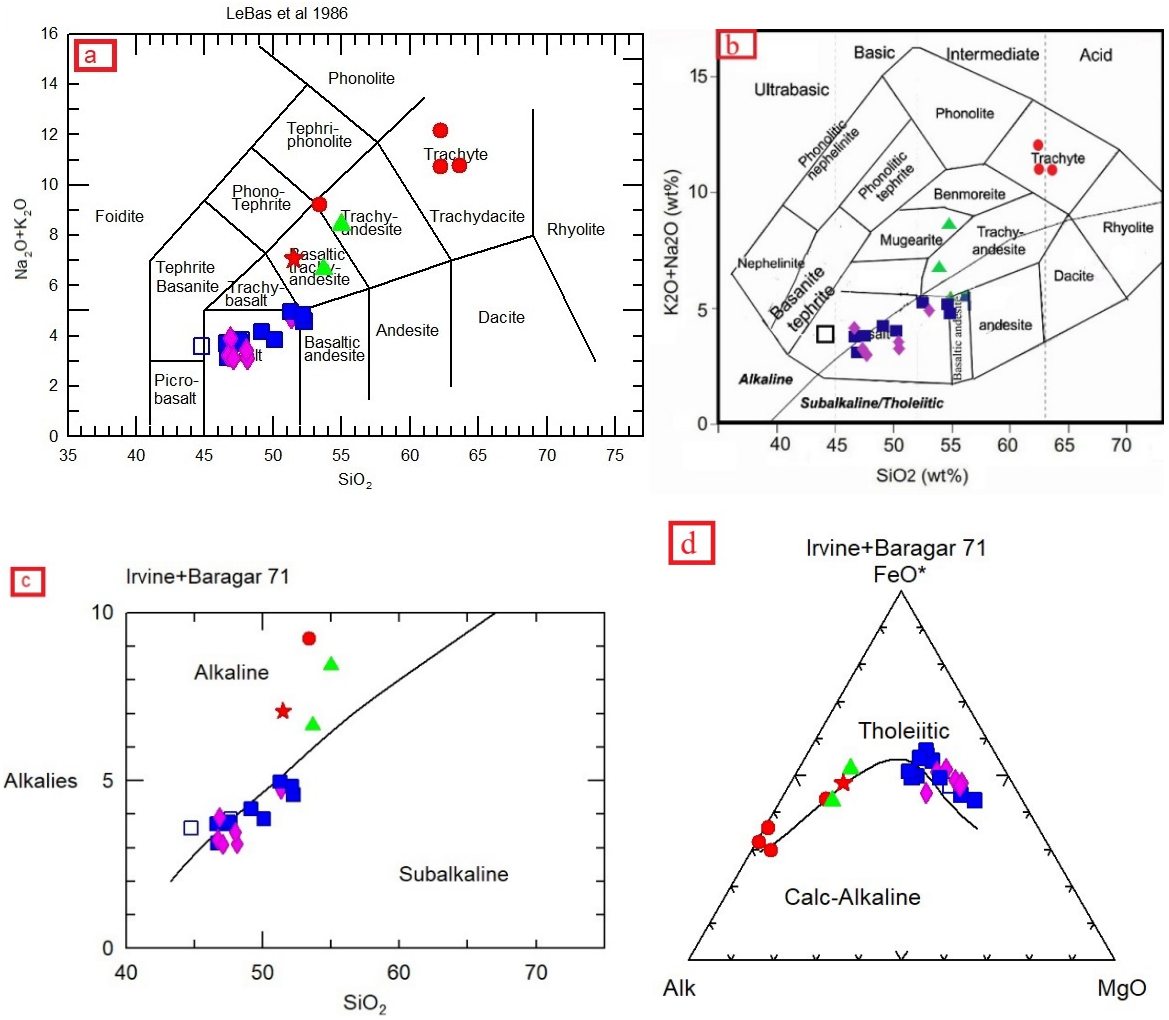

Figure 6. (a) Diagram of $Na_2O + K_2O$ vs SiO_2 (Le Bas et al., 1986). (b) Diagram of $Na_2O + K_2O$ vs SiO_2 (Cox et al., 1979). (c) SiO_2-($Na_2O + K_2O$) diagram (Irvin and Baragar, 1971). (d) FeO*-($Na_2O + K_2O$)-MgO (Cox et al., 1979).

ical properties. In addition, these trends indicate that the main petrological controller was FC in the basaltic magma (Fig. 9). The role of partial melting and FC processes was investigated using pair diagrams of highly incompatible trace elements. In this respect, the ratio of highly incompatible trace element pairs whose segregation coefficients are very similar does not change during differential crystallization but changes slightly during melting (Rollinson, 1993). The general trend of Ni and Co, as two incompatible elements in olivine, and its declination highlight the importance of the early crystallization of this mineral in the basaltic melt. The incompatible element pairs of Ce-La, Nd-Sm, Nb-Ta and Tb-Y have a linear concentration trend, and all pass through the origin of the coordinates of the diagram (Fig. 9). This observation indicates the importance of the petrological process of fractional crystallization with magmatic subtraction in the region (Fig. 9). The Nb/Ta and the Zr/Hf ratios in the rocks of the region are $0.38 - 70$ (average 33.85) and $31.22 - 70.30$ (average 45.87), respectively. In comparison, they are 17.5 ± 0.5 and 36.27 in the primary mantle (Hofman, 1986) and $10 - 11$ and average 33 in crust (Taylor and McLennan, 1985). Besides, the ratio of Nb/U in the primary mantle, continental crust, and ocean island basalt (OIB) is about $10 - 30$ and average 47, respectively (Hofman, 1986), which is 22.98 in the rocks of the study area. Overall, it can be stated that these rocks have originated from a mantle source and have been subjected to magmatic differentiation, and finally contaminated with the continental crust. Changes in the degree of partial melting of samples with low degrees of partial melting indicate a higher concentration of highly incompatible trace elements. Also, with decreasing the degree of partial melting, the ratio of elements with high incompatibility to elements with low incompatibility increases. The elements Y and Zr behavior inconsistently with respect to the main phases in basaltic rocks (e.g., olivine, pyroxene, and plagioclase) such that their Zr/Y ratio $(5 - 20)$ has a positive trend. Besides, with increasing the value of Zr, this ratio increases accordingly. Therefore, increasing the Zr/Y indicates a decrease in the degree of partial melting in the rocks of the study area. Fig. 10a presents the diagram of Nb/Zr changes vs Nb (Marchev et al., 2004) for the region's rocks. The greater concentration of points to reduce Nb/Zr due to the more severe incompatibility of Nb and its relative quantification indicates an increase in relative melting at the origin. Differential crystallization and involvement of CC in the evolution

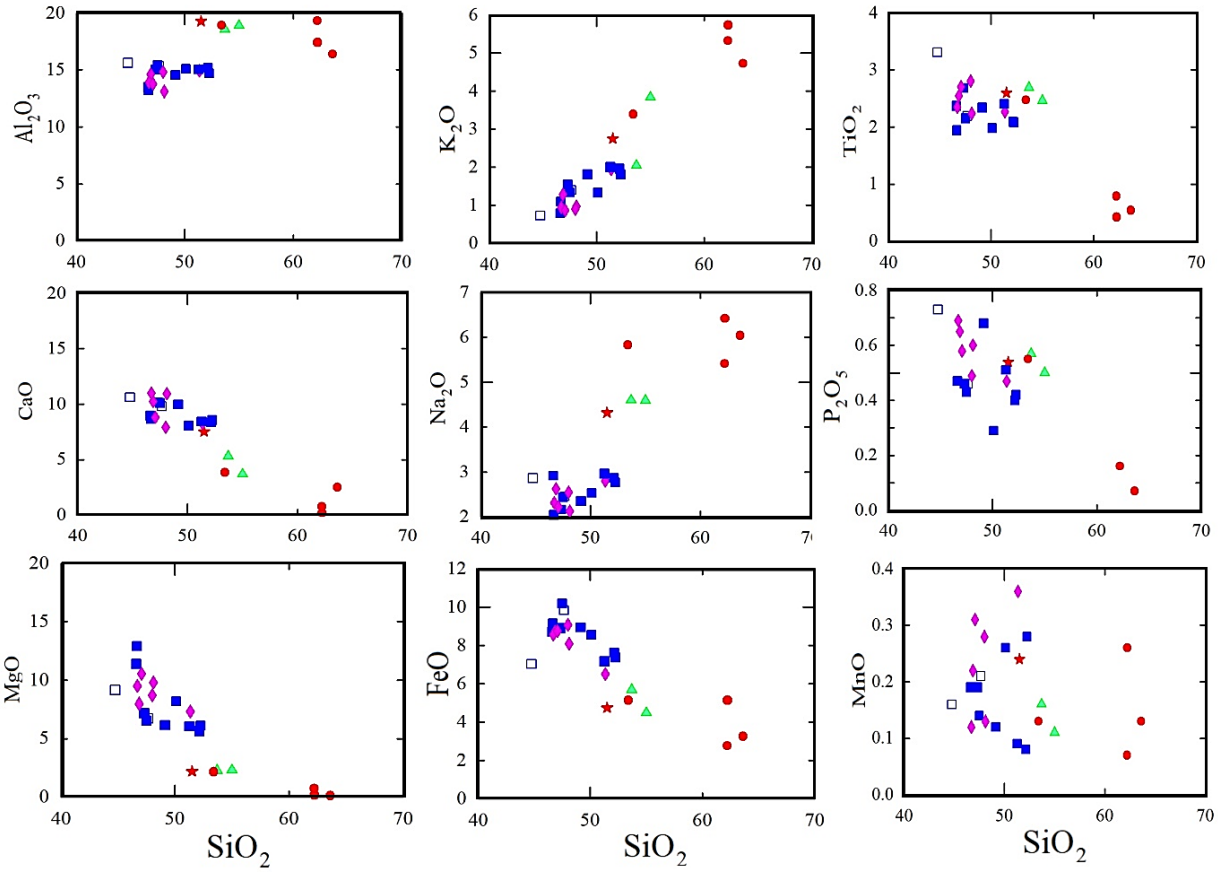

Figure 7. Variation diagrams of the main oxides against SiO_2.

of rocks in the region is shown in Fig. 10 (b).

According to Hart et al. (1989), La/Nb ratio greater than 1.5 and La/Ta ratio higher than 22 indicate magma contamination with crustal compounds. FC is an important factor in basaltic rocks. However, as magma stays in the magma chamber, and with the creation of intermediate rocks (andesite and trachyandesite), in addition to subtraction, to some extent, CC has also been effective. According to Sun and McDonough (1989), the Zr/Nb less than 15.71 and Zr/Y more than 2.46 in the basalts indicate their origination from an enrich source.

Fig. 11 (c) presents the La/Sm and La/Y ratios in normal mid-ocean ridge basalt (NMORB), OIB, lower and upper crust, and middle crust. Based on these ratios, the basalts of the study area are in the range close to the OIB type origin. The placement of the specimens close to the OIB confirms their somewhat enriched mantle source. In addition, the proximity of some samples with the values of different parts of the crust can confirm the role and involvement of CC in the evolution of these basalts. However, most intermediate rocks (e.g., andesite and trachyandesites) show CC. In the Th/Yb vs Ta/Yb diagram (Fig. 11 (b)), the rock samples mostly fall in the OIB range and rarely EMORB, indicating their asthenospheric origin and geochemical characteristics of the intermediate rocks. Besides, the results show the heterogeneity of the magma source making the basaltic rocks of the region (Fig. 10d). The basaltic specimens of the region are mainly located closer to the origin of the OIB, which is derived from the asthenosphere and is somewhat enriched.

In the spider diagrams, the parallel distribution pattern of REEs, their almost constant changes, and the distribution pattern slope are due to the effect of FC in the formation of various basic to intermediate rocks. Sub alkaline basaltic magma can also be formed by 15 to 30% partial melting of upper mantle peridotites (Green, 1973; Green and Ringwood, 2021). Also, the melting at less than 10% can lead to the formation of alkaline basaltic magma (Hirschmann et al., 1998). In fact, due to the greater sensitivity of more incompatible elements to degrees of partial melting, the pattern of REEs decreases with increasing the melting degrees. The parallel form of the REE diagrams of the region's rocks indicates the control of FC and differentiation of the basaltic melt. Intermediate rocks (andesite-trachyandesite) mainly have a higher enriched surface than continental elements, and the distinction between LREE and HREE is more pronounced (Fig. 10 (c)).

In chondrite normalized diagrams, no specific anomaly is observed in Eu, which can be due to the lack of plagioclase and clinopyroxene differentiation (Zeng et al., 2010) during magma evolution. The presence of relatively high amounts of Al_2O_3 in the region's rocks (17.95 wt.%) also confirms the absence of plagioclase in the differentiation phases. However, the Eu segregation coefficients between plagioclase and basalt melt are low under conditions of high oxygen activity, and this element behaves like Eu^{+3} and other REEs (Drake and Weill, 1975). One of the important characteristics of the region's rock samples normalized to chondrite is the gentle enrichment trend of heavy rare

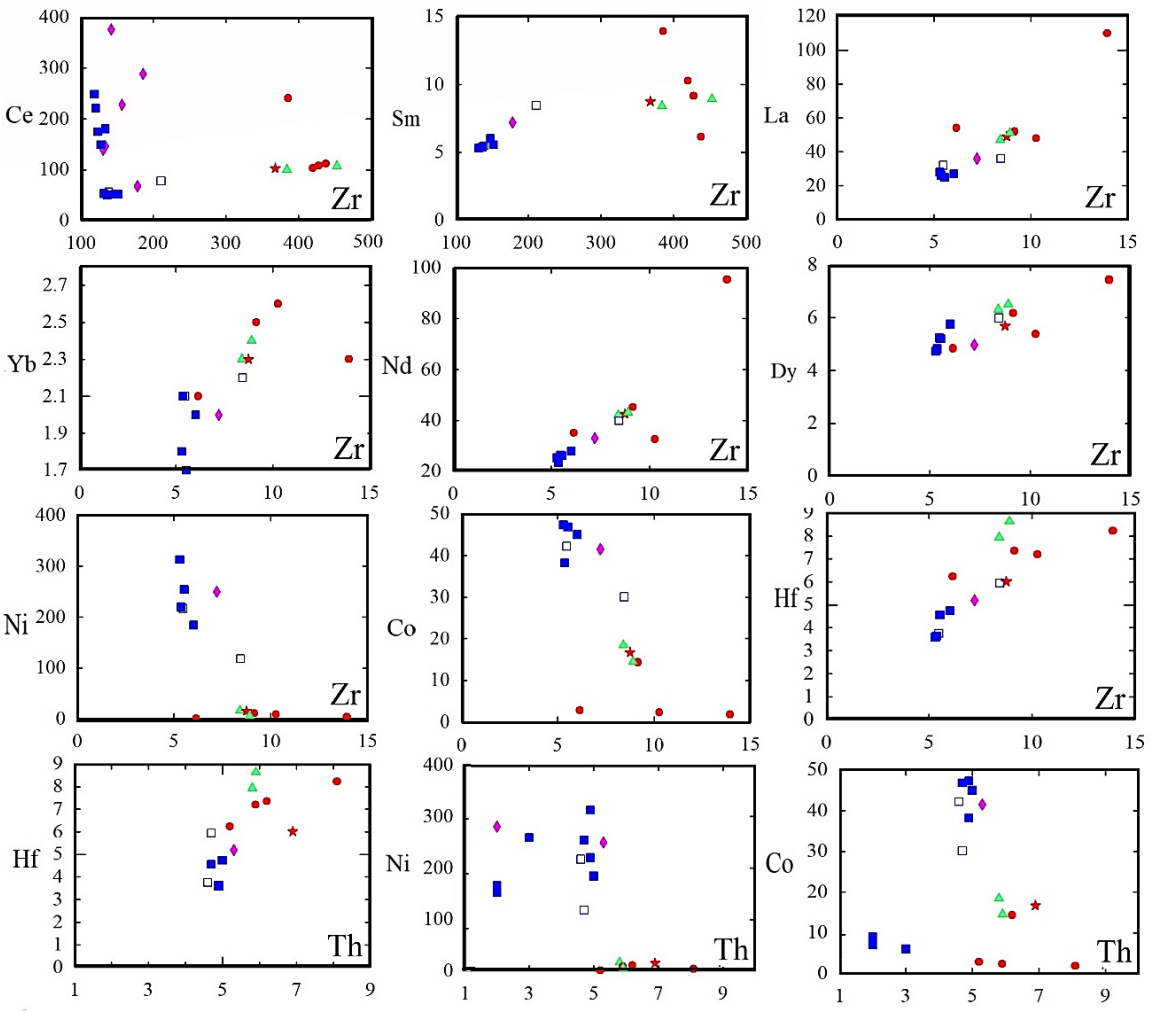

Figure 8. Diagram of changes of rare and rare earth elements vs Zr and Th.

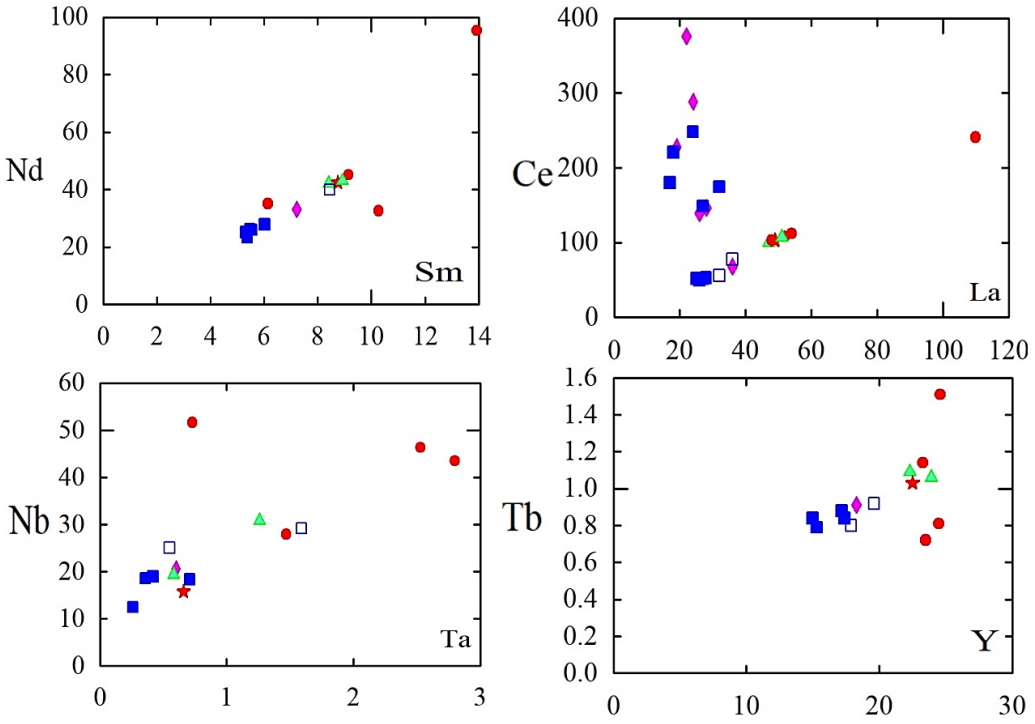

Figure 9. Variations of pairs of strongly incompatible elements Ce-La, Nd-Sm, Tb-Y and Y-Ho.

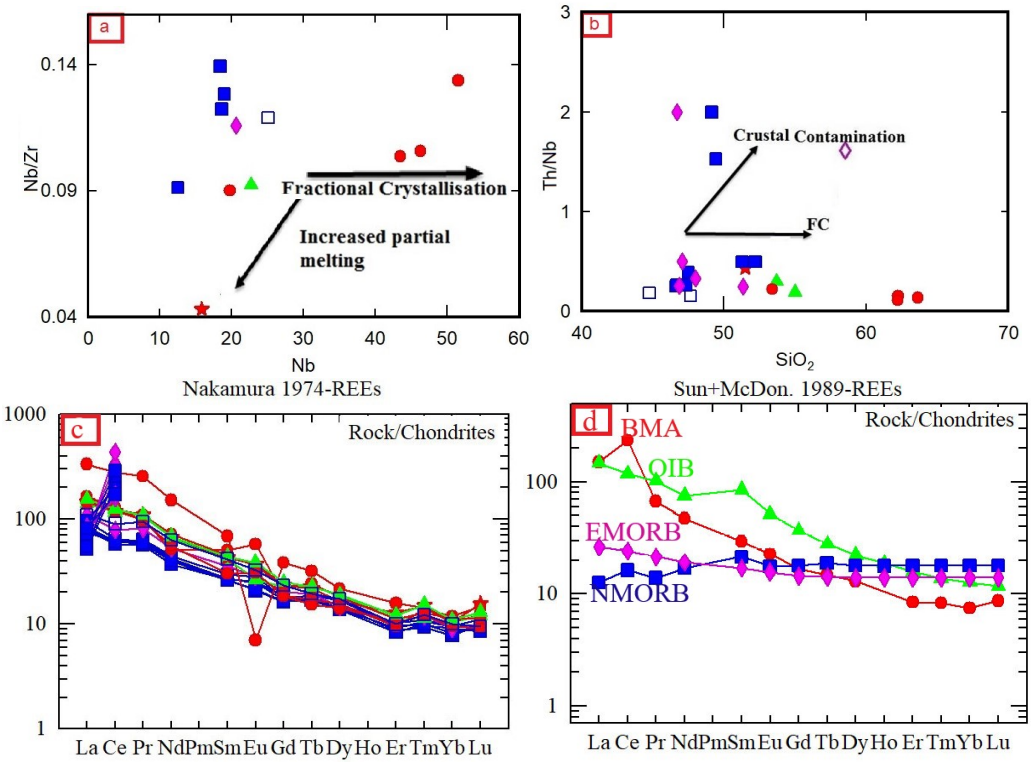

Figure 10. (a) Diagram of Nb/Zr vs Nb (from Marchev et al. (2004)). (b) Diagram of Th/Nb changes against SiO_2 by (Zhang et al., 2012). (c) Spider diagram normalized to chondrite values (Nakamura, 1974). (d) The mean trace and rare earth elements from the region's basalts normalized to chondrite values (**Thampson 1982?**), and primary mantle and MORBs depleted (Sun and McDonough, 1989).

earth elements (HREEs) to light earth rare earth elements (LREES) (Fig. 10 (c)) and the absence of abrupt changes on the curves' slope. As shown in Fig. 10 (c) and Fig. 10 (d), enrichment of more than 10 times LREEs compared to HREEs in most samples indicates a garnet reluctance to enter the melt and its tendency to remain in the mantle origin. According to the spider diagrams of the region's basalts using chondrite, primary mantle, OIB, NMORB, and enriched mid-ocean ridge basalt (EMORB) values (Sun and McDonough, 1989), REE concentrations of these rocks are between EMORB and OIB, and they generally have a similar pattern. Placing the normalized pattern of regional specimens between EMORB and OIB confirms the origin of the basalts from a setting with characteristics between the two origins, both originating from the asthenosphere. The proximity and similarity of the enrichment pattern of regional basalts to OIB compared to EMORB can be a reason for the origin of these basalts from the asthenosphere mantle. Also, OIB-like basalts are generally interpreted as basalts derived from convective asthenospheric mantle or mantle plumes (Zhang et al., 2012). Besides, it is generally accepted that the OIB origin is pure. Despite the general similarity of the pattern of basalts in the region with OIB, the lower concentrations of trace and rare earth elements in the samples of the region should be related to the origin of basalts in the region from a place with slightly less enrichment than OIB, and probably somewhat higher partial melting in the basalts of the region. In the Zr/Y-Ti/Y diagram (Fig. 11 (a)), the altered basalt samples studied fall within the range of within-plane basalts (WPB). These basalts have a higher Zr/Y than other types of basalts. This result indicates an EMORB source for these rocks. This range of melting pressure requires the presence of garnet in the source area. The source area of the magma forming the basaltic rocks was 110 – 100 km in depth. This depth suggests partial melting in a lherzolite garnet source. These results are consistent with those of previous studies. According to the Zr/Y vs Nb/Y diagram (Fitton, 2007) (Fig. 11 (d)), the basalts of our study area are also in the range of OIB type basalts, and their origin is similar to these basalts.

5. Conclusion

Mesozoic igneous rocks in the Alasht-Haraz road, southeast area of Amol city, are mainly consisted of basalt, andesite, trachyandesite, and trachyte volcanic magmas, while hypabyssal dolerite and gabbro rocks are also found occasionally in the region and are closely related to volcanic rocks through their magma origin.

These lavas, which have been mainly erupted in dry environment, are placed over Neocomian rocks and covered with limestone's of Tizkoh Formation from the Cretaceous. Thus, they are inferred to be related to mid to late Neocomian periods.

Based on geochemical studies, these rocks belong to basalt to trachyte ranges. According to petrological investigations, magmas that form basalts are belong to subalkaline series. In fact, basic and intermediate rocks have two origins, as calk alkaline basic magma is produced by partial melt of a peridotite mantle at 25 – 30 Kbar pressure and at the depth of 90 – 100 kilometers with a melting rate of 15 – 30%.

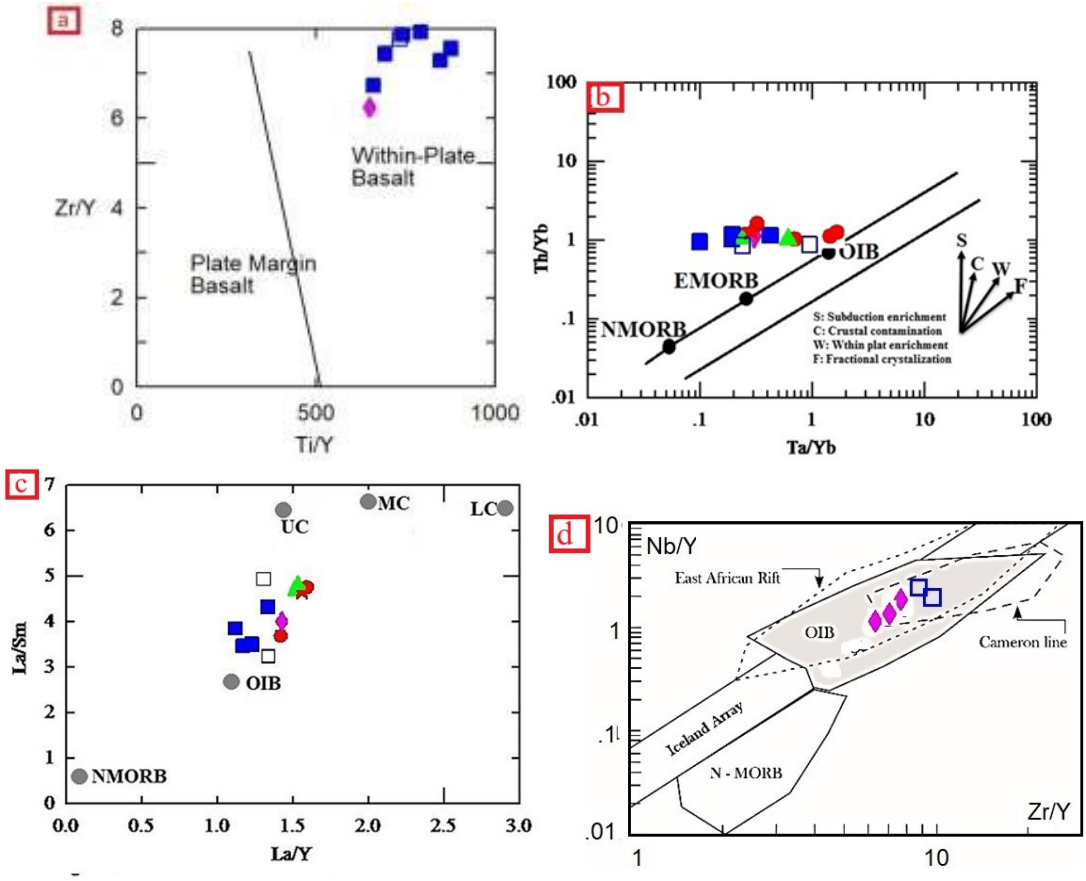

Figure 11. (a) Position of basaltic rocks in the Zr/Y - Ti/Y diagram (Pearce and Gale, 1977). (b) Determining the location of the basalts in the region. (c) Determining the characteristics of the origin of basalts in the region (the values of the upper continental crust (UC) from Taylor and McLennan (1985), the values of the lower continental crust (LC) and the mean continental crust (MC) from Weaver and Tarney (1984), the average MORB from Saunders and Tarney (1984) and Sun (1980), the average OIB of the Sun (1980). (d) Position of basaltic rocks in the Zr/Y vs Nb/Y diagram.

The intermediate magmas forming andesites to trachytes are produced from partial crystallization of the remaining liquid of the deduction of calk alkaline basaltic magma, followed by crust contamination. The increase in the alkalinity of the intermediate magma is related to the entrance of sodium and potassium from the host rock to the rising magma in the crust, since there has been enough time for the entrance of these elements to the remaining liquid from the deduction of basic magma. The maximum rate of increase of alkaline elements is seen in trachytes and trachyandesites. The basaltic magmas under this study are of type of OIB. The decrease in the amounts of rare and rare earth metal elements contents of these rocks can be related to high partial melting degrees of the mantle.

Authors contributions
Authors have contributed equally in preparing and writing the manuscript.

Availability of data and materials
The data that support the findings of this study are available from the corresponding author, upon reasonable request.

Conflict of interests
The authors declare that they have no known competing financial interests or personal relationships that could have appeared to influence the work reported in this paper.

References

Alavi M. (1996) Tectono stratigraphic synthesis and structural style of the Alborz Mountiain system in northern Iran. *Geodynamic* 21:1–33. DOI: https://doi.org/10.1016/0264-3707(95)00009-7.

Arjmandzadeh R., Teshnizi E.S., Ahmadi A.A., Mahdavi A., Tavsoli S., Dabiri R. (2020) The mineralogy, geochemistry and genesis of Aghol-Messi sedimentary copper - uranium deposit, Tabas block, Central Iran. *Researches in Earth Sciences* 11 (4): 47–70.

Ashrafi N., Dabiri R., Jahangiri A. (2024) Some chemical variations in biotite, phlogopite, and muscovite, considering their tectonic setting. *Geopersia* 14 (2): 307–32. DOI: https://doi.org/10.52547/esrj.11.4.47.

Assereto R. (1966) The Jurassic shemshak formation in central Elburz (Iran).

Besse J., Torcq F., Gallet Y., Ricou L.E., Krystyn L., Saidi A. (1998) Late Permian to Late Triassic palaeomagnetic data from Iran: constraints on the migration of the Iranian block through the Tethyan Ocean and initial destruction of Pangaea. *Geophysical Journal International* 135:77–92. DOI: https://doi.org/10.1046/j.1365-246X.1998.00603.x.

Clark G.C., Davies R.G., Hamzepour B., Jones C.R. (1975) Explanatory text of the Bandare Anzali Quadrangle Map 1:250000. *Geol. Surv. Iran,* 19.

Cox K.G., Bell J.D., Pankhurts R.J. (1979) The interpretation of igneous rocks. *George Allen and Unwin,* 450.

Dabiri R., Akbari Mogaddam M., Ghaffari M. (2018) Geochemical evolution and petrogenesis of the Eocene Kashmar granitoid rocks, NE Iran: Implications for fractional crystallization and crustal contamination processes. *Iranian Journal of Earth Sciences* 10 (1): 68–77.

Drake M.J., Weill D.F. (1975) Partitiion of Sr, Ba, Ca, Y, Eu and other REE between plagioclase feldspar and magmatic liqid: an experimental study. *Geochem Cosmochim Acta* 39:689–712. DOI: https://doi.org/10.1016/0016-7037(75)90011-3.

Elmi R., Arin M.A. (2015) Geochemistry and Petrology of Volcanic Rocks in the Alisht Region (Mazandaran). Master Thesis. Islamic Azad University, North Tehran, Iran.

Fitton J.G. (2007) The OIB paradox. *Geological Society of America Special Papers* 430:387–412. DOI: https://doi.org/10.1130/2007.2430(20).

Ghasemi Nejad E.A., Agha-Nabati O., Dabiri R. (2004) Late Triassic dinoflagellate cysts from the base of the Shemshak Group in north of Alborz Mountains, Iran. *Review of Palaeobotany and Palynology* 132:207–217. DOI: https://doi.org/10.1016/j.revpalbo.2004.07.001.

Ghasempour M.R., Ghazi J.M., Biabangard H., Dabiri R. (2015) Petrogenic significance of the Plio-Quaternary Nehbandan mafic lavas, Eastern Iran. *Iranian Journal of Earth Sciences* 6 (2): 133–141.

Gill R. (2010) Igneous rocks and processes: A practical guide. *Wiley-Blackwell,* 428.

Green D.H. (1973) Experimental mantle studies on a model upper mantle composition under water-saturated and water-unsaturated conditions. *Earth and Planetary Science Letters* 19:37–53. DOI: https://doi.org/10.1016/0012-821X(73)90176-3.

Green D.H., Ringwood A.E. (2021) Genesis of the calc-alkaline igneous rock suite. *Contributions to Mineralogy and Petrology* 18:105–162.

GSI (1997) Geological Survey of Iran. Chaloos Geological Map, scale 1:100,000.

Hart W.K., Wolde G.C., Walter R.C., Mertzman S.A. (1989) Basaltic volcanism in Ethiopia: constraints on continental rifting and mantle interactions. *Journal Geophys Research* 94:7731–7748. DOI: https://doi.org/10.1029/JB094iB06p07731.

Hirschmann M.M., Ghiorso M.S., Wasylenki L.E., Asimow P.D., Stolper E.M. (1998) Calculation of peridotite partial melting from thermodynamic models of minerals and melts. I. Method and composition to experiments. *Journal of Petrology* 39:1091–1115. DOI: https://doi.org/10.1093/petroj/39.6.1091.

Hofman A.C. (1986) The relation ship between mantle, continmental crust and oceaic crust. *Earth and Planetary Science Letters* 90 (3): 297–314. DOI: https://doi.org/10.1016/0012-821X(88)90132-X.

Irvin T., Baragar W.R.A. (1971) A guide to the Chemical classification of the common volcanic rocks. *Canadian Journal of earth Science Letters* 8:523–548. DOI: https://doi.org/10.1139/e71-055.

Jenny J., Stampfli G. (1978) Lithostratigraphie du Permien de l'Elbourz oriental en Iran. *Eclogae geologicae Helveticae* 71:551–580.

Le Bas M.J., Le Maitre R.W., Streckeisen A., Zanettin B. (1986) A chemical classification of volcanic rocks based on the total alkali-silica diagram. *Journal of Petrology* 27 (3): 745–750. DOI: https://doi.org/10.1093/petrology/27.3.745.

Marchev P., Raicheva R., Downes H., Vaselli O., Chiaradia M., Moritz R. (2004) Compositional diversity of Eocene-Oligocene basaltic magmatism in the Eastern Rhodopes, SE Bulgaria: implications for genesis and tectonic setting. *Tectonophysics* 393:301–328. DOI: https://doi.org/10.1016/j.tecto.2004.07.045.

Mollai H., R. Dabiri., Torshizian H.A., Pe-Piper G., Wang W.E. (2021) Upper Neoproterozoic garnet-bearing granites in the Zeber-Kuh region from east central Iran micro plate: Implications for the magmatic evolution in the northern margin of Gondwanaland. *Geologica Carpathica* 72 (6): 461–81. DOI: https://doi.org/10.31577/GeolCarp.72.6.2.

Nakamura N. (1974) Determination of REE, Ba, Fe, Mg, Na and K in carbonaceous and ordinary chondrites. *Geochim Cosmochim Acta* 38:757–775. DOI: https://doi.org/10.1016/0016-7037(74)90149-5.

Pearce J.A., Gale G.H. (1977) Identification of ore-deposition environment from trace-element geochemistry of associated igneous host rocks. *Geological Society, London, Special Publications* 7 (1): 14–24. DOI: https://doi.org/10.1144/gsl.sp.1977.007.01.03.

Rollinson H.R. (1993) Using Geochemical Data: Evaluation, Presentation, Interpretation. *John Wiley and Sons,* 325.

Ruttner A.W. (1993) Southern borderland of Triassic Laurasia in north-east Iran. *Geologische Rundschau* 82:110–120.

Saidi S., Tesh R., Javadian E., Sahabi Z., Nadim A. (1997) Studies on the epidemiology of sand fly fever in Iran. II. The prevalence of human and animal infection with five phlebotomus fever virus serotypes in Isfahan province. *American Journal of Tropical Medicine and Hygiene* 26:288–293. DOI: https://doi.org/10.4269/ajtmh.1977.26.288.

Salehpour S., Arian M.A., Rad A.J., Zarei Sahamieh R., Yazdi A. (2025) Geochemistry and technomagmatic environment of Eocene volcanic rocks in Yuzbashi Chay region, west of Qazvin (Iran). *Iranian Journal of Earth Sciences* 17 (1): 1–13. DOI: https://doi.org/10.57647/j.ijes.2025.1701.04.

Sarem M.N., Abedini M.V., Dabiri R., Ansari M.R. (2021) Geochemistry and petrogenesis of basic Paleogene volcanic rocks in Alamut region, Alborz mountain, north of Iran. *Earth Sciences Research Journal* 25 (2): 237–245. DOI: https://doi.org/10.15446/esri.v25n2.74025.

Saunders A.D., Tarney J. (1984) Geochemical characteristics of basaltic volcanism within back-are basins. In: Marginal Basin Geology. *Geological Society of London Special Publication* 16:59–76.

Seyed-Emami K. (2003) Triassic in Iran. Facies 48, 95e106.Sengor, A.M.C., 1984. The Cimmeride orogenic system and the tectonics of Eurasia. *Geological Society of America Special Publication* 195:82. DOI: https://doi.org/10.1007/BF02667532.

Stampfli G., Marcoux J., Baud A. (1991) Tethyan margins in space and time. *Palaeogeography, Palaeoclimatology, Palaeoecology* 87 (1-4): 373–409.

Stampfli G.M., Borel G.D. (2002) A plate tectonic model for the Paleozoic and Mesozoic constrained by dynamic plate boundaries and restored synthetic oceanic isochrons. *Earth and Planetary Science Letters* 196 (1): 17–33. DOI: https://doi.org/10.1016/S0012-821X(01)00588-X.

Streckeisen A. (1979) Classification and nomenclature of volcanic rocks, lamprophyres, carbonatites, and melilitic rocks: recommendation and suggestion of the IUGS, Subcommission on the systematics of igneous rocks. *Geology* 7:331–335.

Stöcklin J. (1974) Northern Iran: Alborz Mountains. In: Mesozoic–Cenozoic orogenic belts: data for orogenic studies. *Geological Society* 4:213–234.

Sun S.H. (1980) Applications of multivariate methods in copper deposit research (in Chinese): Special Issue Math. *Geology* 1:76–89.

Sun S.S., McDonough W.F. (1989) Chemical and isotopic systematics of oceanic basalts: implications for mantle composition and processes. In: Magmatism in the Ocean Basins. *Geological Society, London, Special Publications* 42:313–345. DOI: https://doi.org/10.1144/gsl.sp.1989.042.01.19.

Taylor S.R., McLennan S.M. (1985) The Continental Crust: Its Composition and Evolution- An Examination of the Geochemical Record Preserved in Sedimentary Rocks. *Blackwell Scientific, Oxford,* 312.

Teknik V., Ghods A. (2017) Depth of magnetic basement in Iran based on fractal spectral analysis of aeromagnetic data. *Geophysical Journal International* 209:1878–1891. DOI: https://doi.org/10.1093/gji/ggx132.

Vahdati Daneshmand F. (1999) Geological map of Amol quanderangle. Scale 1:100000. G.S.I.

Vahdati Daneshmand F., A. Karimi (2003) Geological map of Ghaemshar quanderangle. Scale 1:100000. G.S.I.

Weaver B.L., Tarney J. (1984) Empirical approach to estimating the composition of the continental crust. *Nature* 310:575–577.

Zanchi A., Zanchetta S., Berra F., Mattei M., Garzanti E., Molyneux S., Nawab A., Sabouri J. (2009) The Eo-Cimmerian (Late? Triassic) orogeny in North Iran. *Geological Society, London, Special Publications* 312 (1): 31–55. DOI: https://doi.org/10.1144/sp312.3.

Zeng G., Chen L., Xu X., Jiang Sh., Hofmann A. (2010) Carbonated mantle sources for Cenozoic intra-plate alkaline basalts in Shandong, North China. *Chemical Geology* 273:35–45. DOI: https://doi.org/10.1016/j.chemgeo.2010.02.009.

Zhang Y.C., Shen S.Z., Shi G.R., Wang Y., Yuan D.X., Zhang Y.J. (2012) Tectonic evolution of the Qiangtang Block, northern Tibet during the late Cisuralian (Late Early Permian): Evidence from fusuline fossil records. *Palaeogeography,* 350–352. DOI: https://doi.org/10.1016/j.palaeo.2012.06.025.